

PHASE DIAGRAM DETERMINATION USING DIFFUSION MULTIPLES

J.-C. Zhao

Contents

1	Introduction	246
2	Diffusion-Multiple Fabrication	248
3	Analysis of Diffusion Multiples and Extraction of Phase Diagram Data	256
3.1	Imaging Examination and Phase Analysis	256
3.2	EPMA Profiling	257
3.3	Extraction of Equilibrium Tie Lines	259
4	Sources of Errors	266
5	Concluding Remarks	269

1 INTRODUCTION

A diffusion multiple is an assembly of three or more different metal blocks, in intimate interfacial contact, and subjected to a high temperature to promote thermal interdiffusion to form solid solutions and intermetallic compounds [1–5]. It is an expansion of traditional diffusion couples [e.g., 6,7] and the little known “ternary diffusion couples” [8–11]. For the purpose of phase diagram determination, a diffusion multiple is nothing more than a sample with multiple diffusion couples and diffusion triples in it. An example is schematically shown in Fig. 7.1 which has eight diffusion couples (shown by the dotted lines) and four diffusion triples (dotted circles). The local equilibrium at the phase interfaces serves as the foundation to extract phase equilibrium information from diffusion multiples in the same way as that from diffusion couples (discussed in detail in Chapter 6 of this book).

The biggest advantage of the diffusion-multiple approach in phase diagram determination is its high efficiency in both time and raw materials usage. An entire ternary phase diagram can be obtained from a tri-junction region of a diffusion multiple. By creating several tri-junctions in one sample, isothermal sections of multiple ternary systems can be determined without making dozens or even hundreds of individual alloys, thus saving the usage of raw materials. The diffusion-multiple approach can also save the electron probe microanalysis (EPMA) time since there is no need to exchange

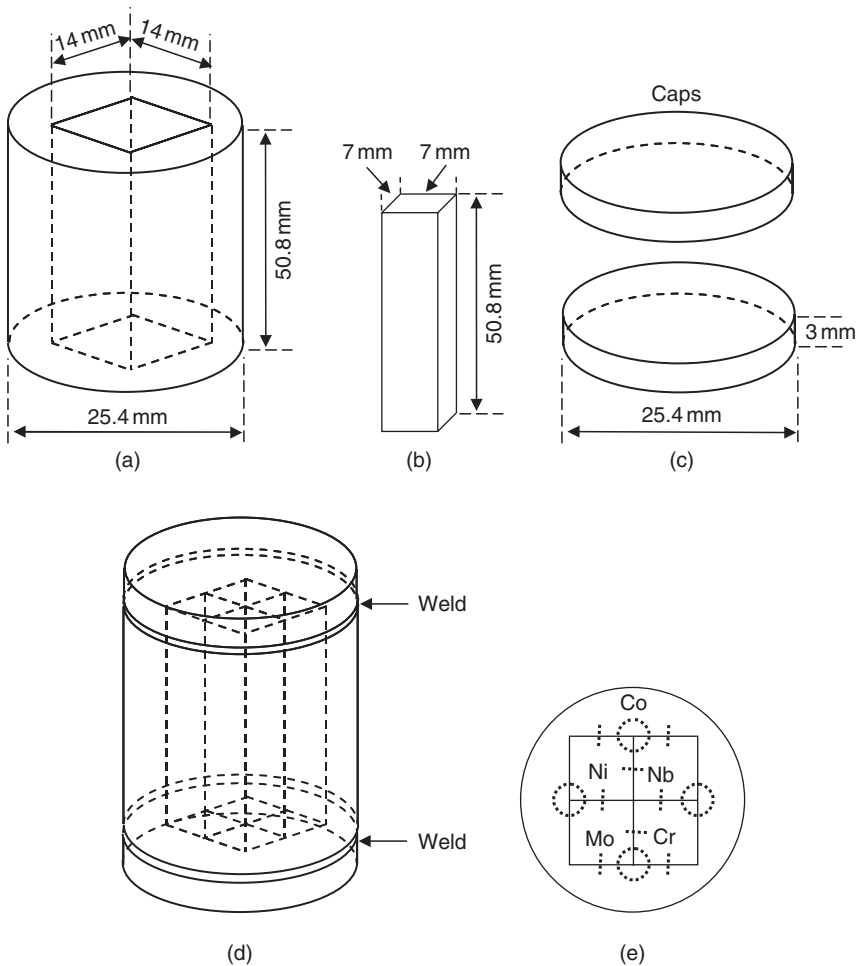


Figure 7.1 Schematic illustration of the components (a)–(c), assembly (d), and cross-sectional view (e) of a Co–Cr–Mo–Nb–Ni diffusion multiple.

many alloy samples in and out of the EPMA system, which is very time-consuming – one needs to wait for a good vacuum to start the analysis each time.

The term “diffusion multiple” was coined to reflect the much expanded capability in recent years in mapping various properties as a function of composition and phases, thus extending the methodology far beyond phase diagram determination. In this sense, a diffusion multiple is primarily used to create compositional variations of both solid solutions and intermetallic compounds to allow their properties to be measured/mapped without synthesizing one composition at a time. Several micron-scale property probes/measurement tools have been developed to enable high throughput measurements of hardness, modulus, thermal conductivity, optical properties, dielectric constants, and other properties. Such property measurements together with the localized composition measurements allow effective construction of

composition–structure–property relationships [1–5]. A review of the state-of-the-art of micron-scale property mapping can be found elsewhere [5].

As part of this book on methods for phase diagram determination, this chapter will only address the phase diagram mapping part of the diffusion-multiple approach. The main topics to be discussed are: (1) how to design and make good diffusion multiples; (2) how to perform effective analyses using EPMA and electron backscatter diffraction (EBSD); (3) how to extract phase diagram data from the EPMA results; and (4) how to take advantage of the diffusion-multiple approach while avoiding its limitations.

2 DIFFUSION-MULTIPLE FABRICATION

The most important step in determining phase diagrams using the diffusion-multiple technique is to make a good diffusion-multiple sample. One needs to spend time upfront to design it with several key considerations as discussed herein. Very successful and less successful examples of diffusion multiples will be used to illustrate these key considerations.

The diffusion multiple shown in Fig. 7.1 was assembled from several components: one cylinder of pure Co (25.4 mm in diameter and 50.8 mm in height) with a 14×14 mm square opening along the cylindrical axis (Fig. 7.1(a)), one prismatic bar each of pure Cr, Mo, Nb, and Ni of $7 \times 7 \times 50.8$ mm dimensions (Fig. 7.1(b)), and two pure Co disks (caps) of 25.4 mm diameter and 3 mm thickness. All the components were cut to shape using wire electro-discharge machining (EDM). The re-cast layer formed on all cut surfaces during wire EDM was removed using grit (Al_2O_3 particles) blast and subsequent mechanical grinding to a metal finish. To make the pieces close to the final dimensions shown in Fig. 7.1, each surface was given a $25 \mu\text{m}$ margin for the loss during grit blasting and grinding of the re-cast layer, that is, the bar inserts of Cr, Mo, Nb, and Ni were cut to the dimensions of $7.050 \times 7.050 \times 50.850$ mm. The pieces were not polished – usually grinding with 1200 grit SiC paper is good enough to make a good diffusion multiple for phase diagram determination. The amount ground away is different for each component/piece and a perfect match among them could not realistically be expected. It is good enough at this stage if the four bar inserts could be fitted into the square opening in the cylindrical Co piece, even though a little loose. It is usually the case that the components are not perfectly aligned, thus the supposed quaternary junction in the center of the diffusion multiple only occasionally yield lots of quaternary phase equilibrium information.

All the pieces were ultrasonically cleaned in acetone or alcohol before assembly. The pure Cr, Mo, Nb, and Ni pieces were put inside the opening in the cylindrical Co bar. Two Co caps were put at the ends of the cylindrical Co bar with the inserts inside, as shown in Fig. 7.1(d). Thin Ni strips were spot-welded onto the Co caps and the Co cylinder to keep the pieces from falling apart during transport to electron beam (EB) welding. The EB welding was performed in vacuum and was performed along the outer circular edges of the Co cylinder, as shown in Fig. 7.1(d). At this stage, the prismatic pieces were still loose inside. The EB-welding step was very important since it kept the inside of the assembly in a vacuum state which would allow the subsequent hot isostatic pressing (HIP) to squeeze all the components together from the outside. The HIP run was performed at 1100°C for 4 h at 200 MPa

argon pressure (the welded Co cylinder and caps served as an HIP can). At 1100°C, the Co was very soft and deformed plastically under the 200 MPa pressure, eliminating the loose gaps among the components and achieving intimate interfacial contacts. The diffusion multiple was then cooled down from the HIP unit, and subsequently wire EDM cut into three equal-height pieces parallel to the Co caps. One such piece of the diffusion multiple was wrapped in Ta foil and sealed in an evacuated quartz tube, back-filled with pure argon. To absorb any oxygen that might diffuse across the quartz tube, some pure yttrium pieces were wrapped inside a Ta foil and put inside the quartz tube before it was sealed off.

The sealed quartz tube with the diffusion-multiple inside was put into an air furnace and heated to 1100°C and held at that temperature for 1000 h. Upon completion of the diffusion annealing, the quartz tube was quickly taken out of the furnace and smashed into a tank of water. The diffusion multiple was thus water quenched to room temperature. It was then ground and polished for optical microscopy and scanning electron microscopy (SEM) examination, followed by EPMA and EBSD.

SEM images taken from the four tri-junctions of the diffusion multiple are shown in Fig. 7.2. The formation of intermetallic compounds, the wide diffusion

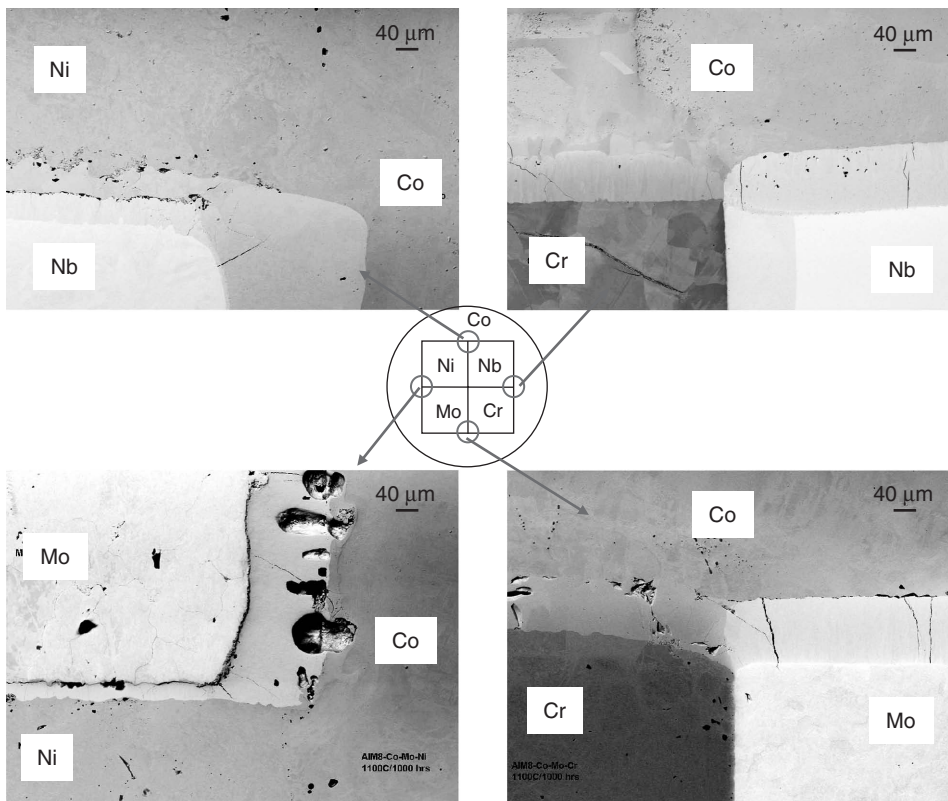


Figure 7.2 SEM images of the four tri-junctions of the 1100°C diffusion multiple shown in Fig. 7.1 showing good interdiffusion and the formation of intermetallic phases between/among the elements. Some of the SEM images were rotated with respect to the schematic diagram shown in the middle.

zones and the good integrity of the sample indicate a very successful fabrication of the diffusion multiple. Detailed analysis of the Co–Cr–Mo tri-junction (lower right in Fig. 7.2) will be described in the next sections of this chapter.

As mentioned earlier, many considerations need to be taken to design and fabricate a successful diffusion multiple. These considerations are discussed here:

- Selection of the components/end members and the annealing temperatures of a diffusion multiple need to be made for the alloy systems of interest. Depending on the temperatures and the compositional regions of interest, one can select pure elements, alloys, or intermetallic compounds as the components of a diffusion multiple. The temperature is an extremely important factor to consider since the diffusion kinetics may be too slow at low temperatures to allow effective interdiffusion to form the phases with sufficient thickness for meaningful analysis. Practically speaking, long-term diffusion annealing should be conducted at a temperature above half of the homologous melting temperature. When a system contains a low melting element or a low eutectic temperature, one can instead select an intermetallic compound or an alloy with high melting point as a component of a diffusion multiple rather than use a pure element as a component. An example is shown in Fig. 7.3 for the Ni–Al–Cr, Ni–Al–Pt, and Ni–Al–Ta systems. Instead of using pure Al as a member of the diffusion multiple, which would limit the annealing temperature to less than 660°C, a Ni–54.5 at.% Al intermetallic compound (B2 NiAl phase) was employed. The use of this intermetallic compound allows the diffusion multiple to be annealed at 1200°C for much faster diffusion. The downside is that only the high-temperature part of the respective phase diagrams can be determined. In this case, this was not a problem since the interest was on the high-temperature Ni-rich regions. Only when pure elements are used, will the entire ternary isothermal sections be obtained.

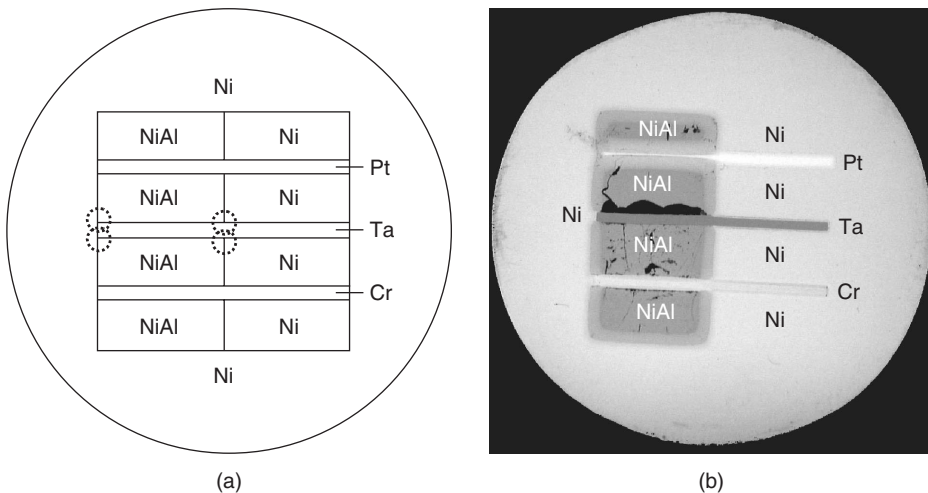


Figure 7.3 The geometry (a) and optical image (b) of a diffusion multiple made up of Ni–NiAl–Pt–Ta–Cr. The diffusion multiple was HIP’ed at 1200°C for 4 h and subsequently annealed at 1200°C for 96 h making the total annealing time at 1200°C for 100 h.

- After selecting the components and the temperatures of annealing, one needs to decide which component will be used as the outer case/matrix of the diffusion multiple (equivalent of an HIP-can). Brittle intermetallic compounds, when used as components of a diffusion multiple, should only comprise the inserts (inner pieces). One advantage of the HIP process in fabricating diffusion multiples is that brittle intermetallics such as NiAl can be easily accommodated as shown in Fig. 7.3. In this case, even though the arc-melted NiAl inserts had a lot of porosity and some small cracks, they were successfully used as components of the diffusion multiple. If no component element is suitable as the outer case, then a separate material can be used as an HIP-can as is the case shown in Fig. 7.4(a) which illustrates a diffusion multiple of Pd, Pt, Rh, Ru inserts within a Cr case/matrix [12,13]. Since the precious metals are expensive, only Cr would be a reasonable choice as the HIP-can. However, Cr is brittle, difficult to weld, and would evaporate rapidly at 1200°C based on vapor pressure data. All these properties prevent Cr from being used as the HIP-can. Therefore, a separate pure Ti HIP-can was used to contain the precious metals and the Cr matrix. Ti is easy to weld using EB, and as an HIP-can it prevents Cr from evaporation (This diffusion multiple was not sliced until after the diffusion annealing to avoid exposing Cr during annealing). One also needs to check the yield strength of the outer shell/HIP-can material to make sure that at the temperature of HIP, the strength is low enough to allow plastic deformation to close the gaps between/among the components inside. This estimation is also important for the design of the outer case/HIP-can dimensions. If the outer case is too thick, it may not deform enough to close the gap at a reasonable HIP time (e.g., 4–8 h) and argon pressure (e.g., 200 MPa). One can increase the HIP temperature to make the materials easier to deform; however, the eutectic temperature or the lowest solidus temperature of the system set the upper temperature limit.
- The next step is to design a geometry for the diffusion multiple. An important consideration is the availability of the raw materials. Some materials are difficult or very expensive to purchase or obtain in large and bulk form; others are readily available. The geometry should be designed to use the smallest amount of the expensive or hard to get materials. For instance, only foils of Pd, Pt, and Rh of 250 μm thickness and a pure Ru piece with two steps on it (500 μm thick on one side and 1000 μm thick on the other) were used to make the diffusion multiple shown in Fig. 7.4(a). Some rough estimation of the diffusion distance using the simple square root Dt (diffusion coefficient D multiplied by time t) calculation is very useful to determine the size (especially thickness) of the components. Again for the case of Fig. 7.4(a), the annealing time was only 40 h at 1200°C due to the very thin (250 μm) foils used to make the diffusion multiple. The diffusion distance during the anneal needs to be constricted to less than the foil thickness. If one does not need the phase equilibrium information of an entire ternary system, one can think of using very thin foils of a very high melting point element within the system as a component of the diffusion multiple. As the high melting point component is consumed by the diffusion process to become alloys with lower melting points, the diffusion may become faster. One needs to pay special attention when two relatively very high melting point elements are side by side, then the diffusion distance may be very small and the bonding between them during

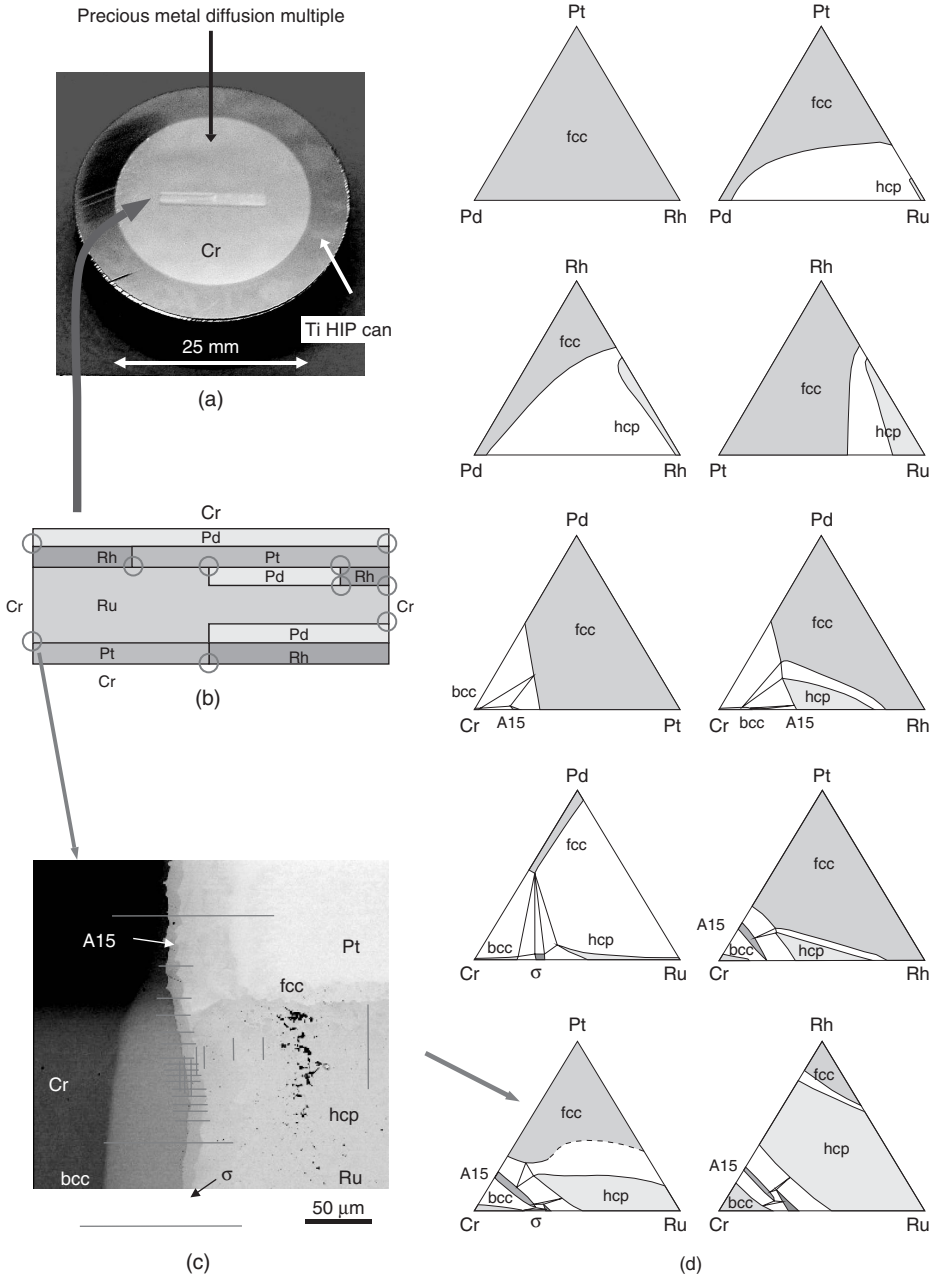


Figure 7.4 A diffusion multiple for rapid mapping of ternary phase diagrams in the Pd–Pt–Rh–Ru–Cr system: (a) optical image of the sample; (b) arrangement of the precious metal foils in the diffusion multiple to create many tri-junctions shown in circles; (c) BSE image of the Cr–Pt–Ru tri-junction showing the formation of the A15 ($\text{Cr}_3(\text{Pt,Ru})$) and σ ($\text{Cr}_x(\text{Ru,Pt})_y$) phases due to interdiffusion of Pt, Ru, and Cr as well as electron microprobe scan locations (lines); and (d) 10 ternary phase diagrams (isothermal sections at 1200°C) obtained from this single diffusion multiple. The phase diagrams are plotted on atomic percent axes with the scales removed for simplicity [12,13].

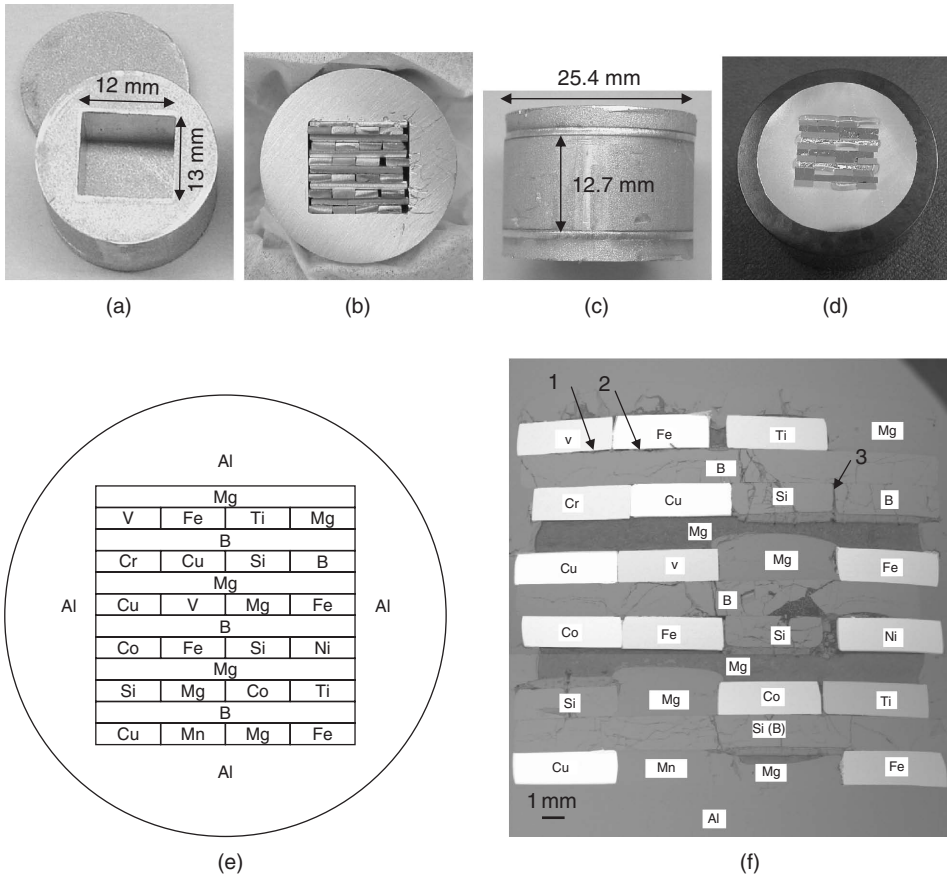


Figure 7.5 A diffusion multiple for Al-based systems: (a) picture of the Al matrix with an 12 mm \times 13 mm opening and Al caps; (b) the assembled diffusion multiple before putting on the Al caps; (c) picture of the diffusion multiple after EB welding of the caps; (d) optical image of the diffusion multiple after HIP'ed at 350°C for 4 h, heat treated at 400°C for 500 h, and then sectioned, ground and polished; (e) schematic diagram showing the arrangement of elements; and (f) low-magnification SEM image showing the various components in the diffusion multiple.

HIP may be very weak, thus preventing any meaningful diffusion reaction. An example is shown in Fig. 7.5 for an Al-based diffusion multiple. The smaller pieces of the elements are 1 \times 3 \times 12.7 mm and the longer pieces are 1 \times 12 \times 12.7 mm. The outer pure Al case/matrix is 25.4 mm in diameter and 12.7 mm in height with an opening of 12 \times 13 mm. After surface preparation, the pieces came in different sizes as shown in Fig. 7.5(b), leaving gaps in various locations. Since many elements are involved, the annealing temperature cannot be much higher than 400°C. In order to give a margin for potential overheating during HIP, the HIP temperature was set at 350°C. At 350°C, Al is soft enough to deform very effectively to close the gaps between/among the elements. However, many elements such as B, Si, V, Fe, Cr, Ni, and Ti have very high melting points relative to the HIP temperature. Not much metallurgical bonding was created between/among these elements during HIP (however, the bonding between pure Al and each of

these elements is relatively good). Gaps between V and B, Fe and B, and B and Si did not close or were created during cooling from HIP temperature to room temperature as shown in locations 1–3 in Fig. 7.5(e). One needs to avoid putting two brittle elements/components side by side, especially if either of them deforms at the HIP temperature (e.g., B and Si do not have any plasticity at 350°C). Diffusion multiples can be made in various shapes and forms as long as an HIP-can can be made to deform effectively at the temperature of interest. When brittle intermetallics such as NiAl are used as a component of a diffusion multiple, it is a good idea to arrange for some equivalent tri-junctions in case one had a crack at the junction. For instance, four equivalent Ni–Ta–NiAl tri-junctions as shown by dotted circles in Fig. 7.3(a), were designed for the diffusion multiple in Fig. 7.3. In this case, the crack, occurring at two locations did not prevent the sample from providing very useful ternary data.

- One also needs to think of how to protect a diffusion multiple from elemental evaporation or an unwanted environmental interaction (e.g., oxidation and pesting). When elements in a diffusion multiple are not prone to evaporation or environmental interaction, one can make a diffusion multiple using HIP and then slice it into several pieces for heat treatment at different temperatures. This will save materials and the effort of making several diffusion multiples. However, when one or more elements in the diffusion multiple is prone to evaporation or environmental interaction, it will be necessary to make one diffusion multiple for each heat treatment temperature. The HIP-can can protect the inside elements from the environment. For instance, a Ti HIP-can was used to protect Cr from evaporation in the diffusion multiple shown in Fig. 7.4. The diffusion multiple was not sliced to pieces for different temperatures. A sliced diffusion multiple of Ni–NiAl–Ta–W–R88 (Rene 88) was destroyed, Fig. 7.6, after being annealed at 700°C for 4000 h. Even though the diffusion multiple was wrapped in Ta foil and yttrium pieces to absorb oxygen during heat treatment were placed inside the sealed quartz tube back-filled with pure Ar, apparently enough oxygen diffused across the quartz tube to cause severe pesting reaction of the Ta and W. There were significant forces built up during the pesting to deform the cylindrical sample into the shape pictured in Figs. 7.6(a) and (b). All the metallic Ta and W pieces were gone. If the diffusion multiple had not been sliced, the R88 outer case/HIP-can would have been able to protect the Ta and W from pesting.
- One additional consideration in making a diffusion multiple is whether to quench or furnace cool the sample from the diffusion annealing temperature to room temperature for analysis. A quenched sample is more likely to retain the high-temperature equilibria to room temperature, but it may promote more cracking of the brittle intermetallic phases. Slow furnace cooling may reduce cracking, but it may result in phase precipitation to complicate the analysis. Quenching is recommended unless it is not possible to do so or unless the cracking is very severe. For instance when the diffusion heat treatment is performed in a conventional vacuum furnace, it is difficult to quench the sample into water.

Upfront considerations of the above points can dramatically increase the success rate of any diffusion multiple fabrication. The EB welding and HIP processes are very convenient steps for making diffusion multiples. The HIP process has been effectively

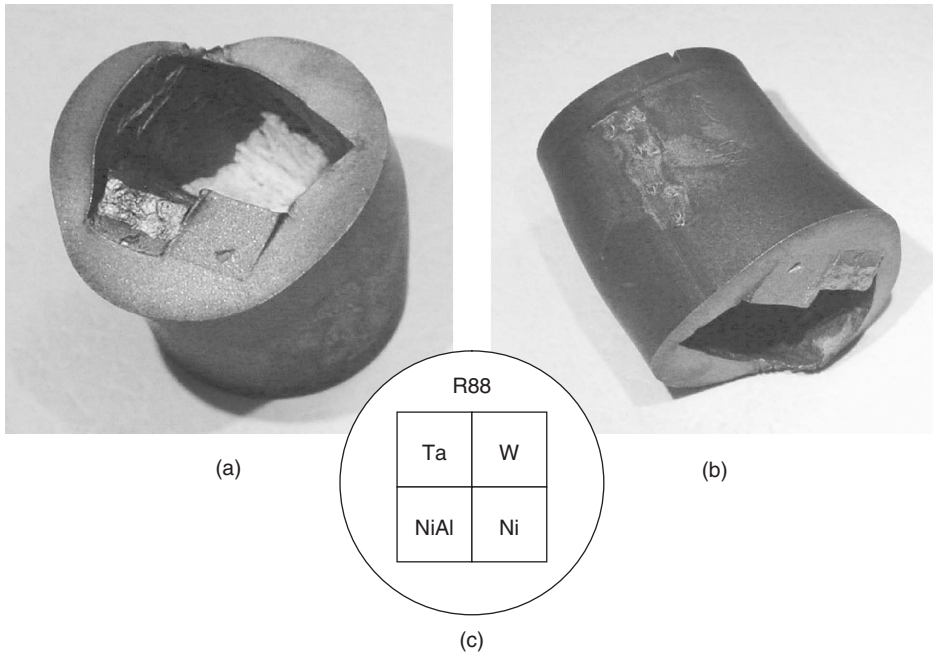


Figure 7.6 An unsuccessful diffusion multiple due to a pesting reaction: (a) and (b) pictures (taken at different angles) of the Ni-NiAl-Ta-W-R88 (Rene 88) diffusion multiple after annealing at 700°C for 4000 h; and (c) schematic cross-sectional view of the diffusion multiple.

used to make many successful diffusion multiples. With a good design, the HIP process makes it possible to include many binary diffusion couples and ternary diffusion triples into a diffusion multiple. The HIP process also helps to crack any surface oxide such as Al_2O_3 to make intimate interfacial contacts for interdiffusion reactions.

Determination of the low-temperature part of a phase diagram containing only high melting point elements, for example, a 500°C isothermal section of a Co-Cr-Mo system, is very difficult using equilibrated alloys; it is even harder to do so using diffusion couples and multiples. It is impractical to promote sufficient interdiffusion at such low temperatures to form the intermetallic compounds and solid solutions to determine equilibrium phase diagrams. A two-step process can be employed to determine phase diagrams at relatively low temperatures. One can first anneal a diffusion multiple at a high temperature (above half the homologous melting point), and then anneal it at low temperatures of interest to examine the phase precipitation. In such studies, the high-temperature annealing serves the purpose of creating the compositional variations/intermetallics, that is, creating many alloys simultaneously. The process also serves, in a sense, as an equivalent to the homogenization annealing of equilibrated alloys. The low-temperature annealing would be the equivalent of heat-treating many alloy compositions at the temperature of interest to examine their phase formation and equilibria. Theoretically, with such a process it should be possible to obtain the isothermal sections at relatively low temperatures. The analysis process is non-trivial for complex systems. A combination of diffusion multiples with a few selected alloys is highly recommended.

3 ANALYSIS OF DIFFUSION MULTIPLES AND EXTRACTION OF PHASE DIAGRAM DATA

3.1 Imaging Examination and Phase Analysis

The Co–Cr–Mo ternary system in the diffusion multiple shown in Fig. 7.1 will be used to illustrate the key processes analyzing a diffusion multiple and extracting phase equilibrium data. Since most diffusion multiples contain brittle intermetallic phases, it is very important to cut, grind, and polish the samples very carefully. Even so, cracking of the intermetallics is often unavoidable. As long as the cracking is not at critical locations, one can get lots of phase equilibrium data from a diffusion multiple.

Simple optical microscopy is usually used first to examine the phase formation and the integrity of a diffusion multiple. Most phases can usually be seen with an optical microscope, although sometimes it is hard to tell which one is which when many phases are present. Optical examination from low magnifications to high magnifications along with information on the existing binary phase diagrams can give clues of the phases present. After optical examination, SEM is often performed to obtain backscattered electron (BSE) images such as those shown in Fig. 7.2. The atomic number contrast along with some energy dispersive spectroscopy (EDS) analysis (which is often available with SEM) can help to further define some or most of the phases. Note that sometimes the contrast from different grain orientations can confound the atomic number contrast. A high quality and high contrast BSE image provides lots of good information about the phases and related equilibria.

EBSD is a very useful tool to perform crystal structure analysis to aid phase identification [14–16]. EBSD can be used to identify crystal structures of micron-size phases in a regularly polished sample (without going through the trouble of making transmission electron microscopy (TEM) thin foil specimens). Commercial EBSD systems are available as an attachment to regular scanning electron microscopes. As a focused EB impinges on a phase, it generates BSEs in addition to secondary electrons, Auger electrons, X-rays and others. The BSEs escaping the sample are further scattered/diffracted by the crystal lattice, thus producing a spatially resolved intensity variation. When a phosphor screen or another type of detector is used to capture the BSEs, a pattern (similar to a Kikuchi map in TEM) is obtained. Sophisticated algorithms have been developed to automatically capture and index the EBSD patterns [16]. The sample is usually tilted at about 60–70° to face the EBSD detector to maximize the collection of diffracted BSEs.

From a phase diagram mapping standpoint, EBSD is important to detect phase boundaries and identify phases, and is critical to efficient experimental planning in the “identification” and “screening” activities. If a list of expected phases in a sample can be generated, then EBSD can be used to rapidly detect the spatial positions of the phase boundaries on the diffusion multiple. The spatial positions of these phase boundaries can be directly related to the quantitative compositions measured by the EPMA, resulting in phase boundary positions on the phase diagram. Phase identification is accomplished by a direct match of the diffraction bands in an experimental EBSD pattern with simulated patterns generated using known structure types and lattice parameters. In this regard, all known crystal structures of a system should be put into the EBSD system software. For instance, the Cr–Pt–Ru ternary system has five

phases: bcc, fcc, hcp, A15 (Cr₃Pt), and (Cr–Ru) σ phase (Fig. 7.4(c)). Their crystal structure data (space group, atom positions, and lattice parameters) are provided based on crystal structure information from the three binaries: Cr–Pt, Cr–Ru, and Pt–Ru [17]. When ternary intermetallic compounds are known from crystal structure databases, their crystal structure information should also be provided. In the Cr–Pt–Ru case, no ternary compounds were reported. All the EBSD patterns from the Cr–Pt–Ru system belonged to the five known structures. The EBSD analysis greatly helped locate the interface between the A15 and the σ phases – the SEM image alone cannot differentiate them (Fig. 7.4(c)). An EBSD phase map of this same area locates the positions of the phase boundaries (especially the A15/ σ phase boundary), which were used for intelligent placement of EPMA scan locations.

The power of EBSD is its capability for effective crystal structure identification with a micron-scale resolution yet without laborious sample preparation. Polished metallographic samples are usually good for analysis with only one additional step. Most metallographic procedures finish polishing with a 1 μm diamond medium. This finishing step leaves a damage layer on the surface on the order of 0.5–1 μm , particularly for metallic samples. This level of surface damage can severely degrade the quality of EBSD patterns due to the shallow depths (~ 100 nm) of beam interaction. To relieve this surface damage, vibratory polishing with a 0.05 μm silica suspension for several hours is suggested. For diffusion-multiple samples, too many hours' vibratory polishing can induce topographic relief due to the differences in hardness among different components/elements. Such relief is undesirable for EPMA analysis. A trial and error method can be used to select a balanced time. Usually a few hours are a good starting point.

If a completely unknown ternary compound should appear, the EBSD technique may not be the best way to identify it effectively. X-ray or TEM work would be preferred for detailed crystal structure identification. In a sense, all crystal structure identification (including EBSD, X-ray diffraction (XRD), and electron diffraction in TEM) of an unknown phase is more or less a matching game. In other words, one needs first to identify which crystal system it belongs to (fcc, bcc, tetragonal, etc.) and then gradually identify the detailed space group.

If most of the phases can be identified from the diffusion multiple using optical microscopy, SEM and EDS analysis, and EBSD, one can construct a rough topology of the phase diagram without the phase boundaries being accurately defined. Since the usage of all these tools is less expensive than EPMA, as much upfront analysis should be performed using them to define the locations of phases, their interfaces and tri-phase junctions. This information is then used to most effectively place the EPMA line scans onto the sample (or the corresponding BSE image) such as those shown in Figs. 7.4(c) and 7.7.

3.2 EPMA Profiling

The EPMA (or microprobe as it is usually called) is an essential and powerful tool to analyze diffusion multiples. EPMA is a technique capable of chemically analyzing the composition of a solid with high spatial resolution and sensitivity [18–20]. The volume excited under typical EPMA conditions is on the order of a cubic micron. EPMA can detect elements spanning most of the periodic table, from Be to U, with typical detection limits of 0.1% atomic.

EPMA is naturally well suited to achieving efficient and accurate composition profiling with high spatial resolution. The marriage of high-speed computer automation and very precise sample stage and X-ray spectrometer hardware has provided a powerful analytical tool. Modern EPMA systems are usually equipped with a motorized stage that has a positional precision of $0.5\ \mu\text{m}$ in the *X*-, *Y*-, and *Z*-directions, and can move over a range of several centimeters. Such a system allows automated data collection by advance logging of the EPMA line scan positions such as those shown in Figs. 7.4(c) and 7.7 into an executable file that allows the instrument to collect data without the presence of the operator.

Since EPMA machine time is usually expensive, it is very important to achieve very high throughput EPMA while maintaining acceptable accuracy and precision in the resultant compositions measured. In measuring large numbers of phases and intermetallic compounds with compositions varying only slightly among some of them, one needs to carefully select the analysis parameters that would give the most productive results. A large effort should be placed on both qualitative and quantitative examination of diffusion multiples in advance of more thorough quantitative profiling in order to balance the accuracy needed with the total acquisition time during analyses of up to a few thousand data points per ternary system. Usually the EPMA analysis is performed on the order of 1 min per point.

The main procedures for automating the electron microprobe effort can be broken down into four activities: identification, screening, analysis design, and acquisition. The “identification” activity involves a combination of light optical and backscatter electron imaging coupled with some form of qualitative analysis to distinguish meaningful regions from artifact (topographic or crystallographic differences) and so confirm/gauge the information obtained during imaging or phase analysis as described in Section 3.1. Sometimes, more than one section of a specific multiple needs to be analyzed due to porosity, cracking of intermetallic compounds during sample preparation, or other deleterious effects along a particular binary or ternary region in a given metallographic section.

The phases identified by BSE contrast would be compared to adjacent regions using semi-quantitative surveys to determine presence of unique phases or diffused regions that could not be clearly defined in previous imaging efforts – a critical step to avoid spending hours performing unnecessary quantitative analysis. This was often done using X-ray counting integration for specific elements present over a pre-set time, or by performing an EDS spectral acquisition on the areas for comparison. In some cases a quick wavelength dispersive spectroscopy (WDS) count rate meter comparison was used. This “identification” activity allows the locations of all significant phases in the diffusion multiple to be logged into the computer.

The “screening” activity includes using EDS, WDS, or both for semi-quantitative and quantitative analysis. The key is to obtain a matrix of count rates from identified phases for the elements present. Typically screening was performed in an automated mode and analysis was done over a very small subset of the actual analysis matrix to approximate the composition ranges to be measured. This gives vital information to allow the selection of all analysis parameters.

In the “analysis design” activity, the goal is to optimize all the conditions for the impending analyses. The primary EB energy, beam current, choice of standards, spectrometer crystals, detector bias, and pulse height discrimination must be

selected from results of the abbreviated “screening” trials. It must be made certain that the statistical accuracy required in crucial regions is met and that a pre-determined number of composition profiles are tested to “map” the diffusion multiple most efficiently. Also important here are X-ray counting times, dead time error, detection limits, and the accuracy required. The “step size” (distance between points along a profile) is an extremely important parameter during EPMA analysis. To increase the step size from 1 μm to 2 μm will cut the EPMA run time in half. However, some regions with very thin phases may be missed during a 2 μm step run. One solution to this is to segment a scan into multiple sections with different step sizes, for example, 1 μm for thin phase regions and larger steps for thick and large phase regions. Since the acquisitions are performed in an automated fashion, one can alter specific sections of the acquisition to accommodate needs of greater sensitivity, counting time on peak and background positions, etc. as a function of the composition ranges.

The “acquisition” activity includes intermittent analyses of the standards as a measure of the “drift” of beam current, stage, spectrometer position, and other instrument stability issues. This can help salvage data by correcting acquired values using known variation from the standard. It also helps identify long-term stability limits.

Due to the large number of data points collected for a given EPMA acquisition, the challenge is to minimize the X-ray counting times at each data point. A few unnecessary seconds spent counting at each data point represent many hours of acquisition time for typical EPMA runs on diffusion multiples.

Having some knowledge of the approximate levels of elemental concentration within a phase and along a gradient to be measured is extremely important in making decisions about the counting statistics and dwell times needed for each measurement for all elements and for both peak and background X-ray integrations.

All the information collected from the preliminary analyses is used to effectively place the EPMA scans onto a diffusion multiple as shown in Fig. 7.7 for the Co–Cr–Mo ternary system and to select the optimum step size(s) for each scan. EPMA analysis can then be performed to obtain compositions of the points along these scans. Compositions of a total of 1557 points were collected for the Co–Cr–Mo ternary system.

3.3 Extraction of Equilibrium Tie Lines

Note there are usually no two-phase mixture regions in diffusion multiples – two-phase mixtures are thermodynamically forbidden for binary diffusion couples. Even though two-phase mixtures are allowed by thermodynamics for ternary systems, they seldom appear in the diffusion annealing process. Two phases reach local equilibrium at an interphase interface; and three phases reach local equilibrium at a tri-junction.

As the EPMA beam travels at a specified step size along a line scan across different phases, the composition of each point is obtained. Since the beam hits single-phase regions far more often than an interphase interface, the population density of data inside a single-phase region should be much higher than that of two-phase regions in the phase diagram. Only when the EPMA point is at or near an interphase interface – while sampling X-ray signals from both phases, will a composition inside a two-phase region in the phase diagram be obtained. Therefore, when the compositions of points in an EPMA scan are plotted onto an isothermal section (similar

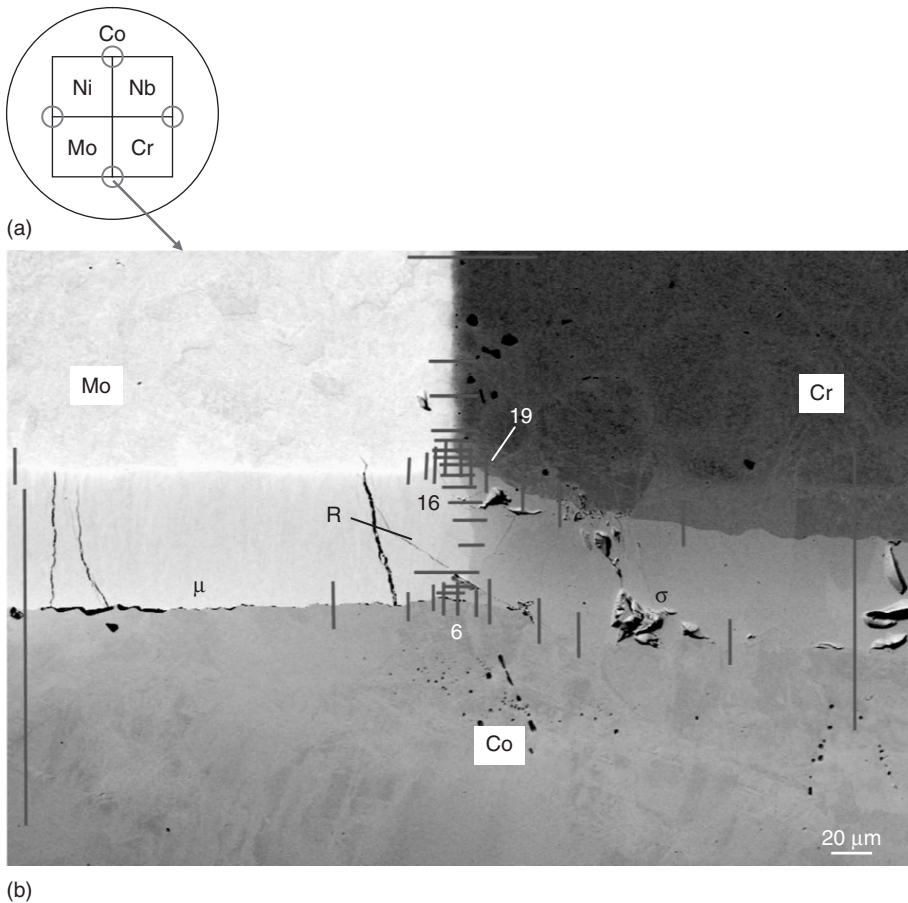


Figure 7.7 Schematic diagram (a) of the diffusion multiple shown in Fig. 7.1 and the EPMA line scan positions marked onto a BSE image (b) of the Co–Cr–Mo tri-junction.

to a diffusion path), the EPMA data are close together in the single-phase regions and scarce in the two-phase regions. In addition, as the EPMA beam moves from one side of an interphase interface to another, the compositions of the two phases should be on a straight line.

By simply plotting the at.% Mo concentration against the at.% Cr concentration of all the 1557 data points obtained from line scans shown in Fig. 7.7(b) in a triangular plot (i.e., on an isothermal section) without any data reduction/processing, one can see a good distribution of data points across the entire ternary isothermal section, Fig. 7.8(a), which indicates that the EPMA line scans are well positioned/placed. By connecting all the data points together for each EPMA scan, one can see the behavior discussed above: densely populated points in single-phase regions and a few data points along a straight line in two-phase regions. Thus, the approximate phase boundaries can be estimated by looking at the density and alignments of data points, Fig. 7.8(b), especially when the binary phase diagram information is used to help bracket the phase regions along the edges of the isothermal section.

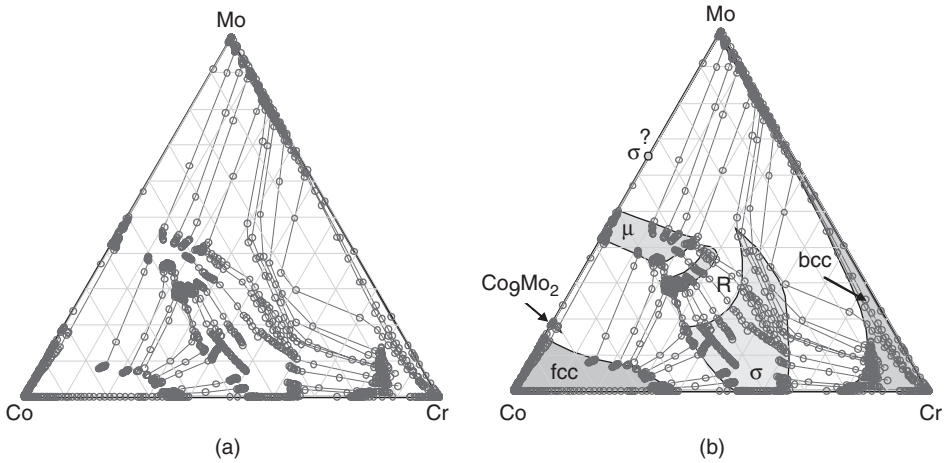


Figure 7.8 Plots of at.% Mo concentration against at.% Cr concentration in a triangular format for all the EPMA data collected for the Co–Cr–Mo ternary system: (a) plot of all data without any data reduction/processing and (b) estimated phase boundary locations based on knowledge of the related three ternary systems and the ternary R phase.

The right-hand edge of Fig. 7.7(b), far from Mo, is essentially a binary diffusion couple of Co and Cr. The solubility of Co in Cr and Cr in Co and the composition range of the σ phase are all consistent with the binary phase diagram [17]. Moving from the right-hand edge gradually toward the center of Fig. 7.7(b), more and more Mo diffuses into the fcc Co phase, the σ phase, and the bcc Cr phase, thus tie-lines with higher and higher Mo concentrations are obtained as shown in Fig. 7.8(b). It can be seen that Mo partitions higher in the σ phase than in the fcc and bcc phases. The top edge of Fig. 7.7(b), far from Co, is essentially a binary diffusion couple of Cr and Mo. Cr and Mo are mutually soluble, forming a continuous bcc solid solution. Moving from the top edge gradually toward the center in Fig. 7.7(b), more Co is diffused into the bcc phase. Similarly, the left-hand side of Fig. 7.7(b), far from Cr, is essentially a diffusion couple of Co and Mo. There is about 15 at.% solubility of Mo in Co and low solubility of Co in Mo, all consistent the existing binary Co–Mo phase diagram [17]. Both the μ (Co_7Mo_6) phase (called ϵ phase in recent phase diagram compilation [17]) and the Co_9Mo_2 phase were observed. The Co_9Mo_2 phase is hard to see in Fig. 7.7(b), but can be clearly seen in a high contrast BSE image taken from a binary Co–Mo region of the diffusion multiple, Fig. 7.9. There are contradictory reports concerning the stability of the σ phase in the Co–Mo binary system. Quinn and Hume-Rothery observed the eutectoid decomposition of the σ phase at $\leq 1250^\circ\text{C}$ [21], whereas Heijwegen and Rieck observed the σ phase formation in Co–Mo diffusion couples annealed at 1000°C for 48 h [22]. The absence of the σ phase in the binary Co–Mo diffusion couple region shown in Fig. 7.9 is consistent with the result of Quinn and Hume-Rothery. Moving from the left-hand edge gradually toward the center, more Cr has diffused into the μ , bcc, and fcc phases and a bit into the Co_9Mo_2 phase. At the center of the tri-junction, all three elements interdiffused to form the ternary compositions and a ternary compound, the R phase that can

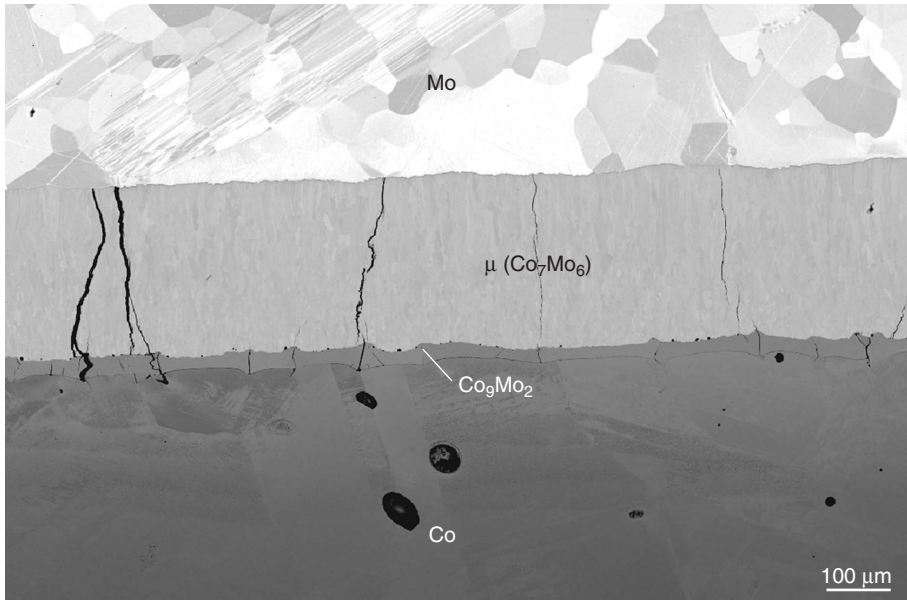
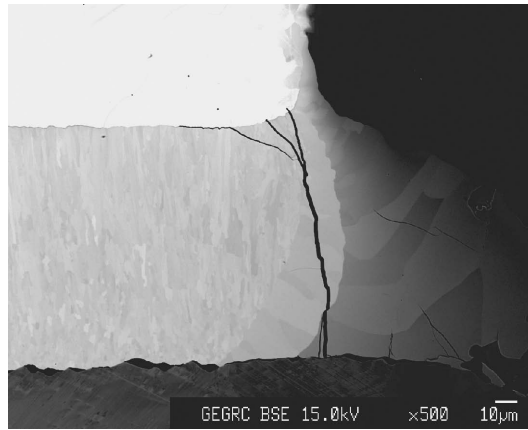


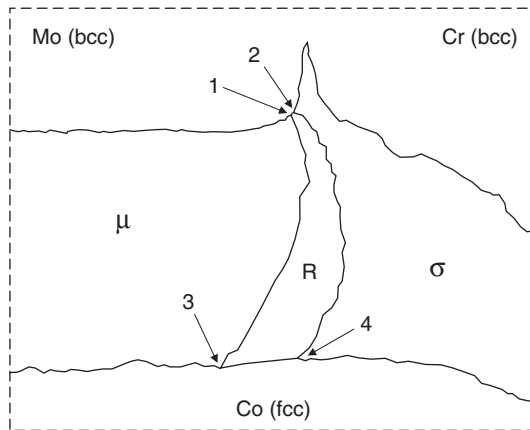
Figure 7.9 SEM BSE image of a Co–Mo binary region of the diffusion multiple shown in Fig. 7.1 annealed at 1100°C for 1000 h, clearly showing the formation of the μ phase and the Co_9Mo_2 phase and the absence of the σ phase. The bcc Mo phase shows a strong orientation contrast.

be seen in a high contrast BSE image shown in Fig. 7.10. The arrangement of the R phase in relation to other phases in Figs. 7.10(a) and (b) created tri-junctions 1–4 that indicates the existence of the corresponding four three-phase triangles: $\text{bcc}(\text{Mo}) + \mu + \text{R}$, $\text{bcc}(\text{Mo}) + \text{R} + \sigma$, $\text{fcc}(\text{Co}) + \mu + \text{R}$, and $\text{fcc}(\text{Co}) + \text{R} + \sigma$.

During EPMA data reduction to extract equilibrium tie lines, it is very beneficial to make two plots for each EPMA scan, as shown in Fig. 7.11 for a scan (scan #16 in Fig. 7.7(b), from right to left) that started in the σ phase, crossed the R phase, and ended in the μ phase. The first plot, Fig. 7.11(a), shows the compositions of individual points against location (distance in X -direction). This helps to extrapolate to the local equilibrium compositions at the phase interface (Fig. 7.11(a)). The simple straight line extrapolation to the phase interface between the μ phase and the R phase can result in reasonable values for the equilibrium tie line between the two phases (Fig. 7.11(a)). However, since the Cr and Mo concentrations of the σ phase vary quickly with distance, it is hard to extrapolate reliable tie-line compositions, especially since it is not known whether linear extrapolations are still valid. The second graph plots one element (Mo) against another (Cr) (Fig. 7.11(b)). This plot basically shows the compositional path of the scan in the corresponding phase diagram. Since the tie line must be a straight line passing through the two-phase region and also passing through any points along the path inside the two-phase region, this graph can be used to define the tie lines very quickly, as shown by the heavy dotted lines in Fig. 7.11(b). Both plots are very important for the extraction of equilibrium tie lines.



(a)



(b)

Figure 7.10 SEM BSE image (a) and a corresponding schematic (b) of the Co–Cr–Mo trijunction of the diffusion multiple shown in Fig. 7.1 annealed at 1100°C for 1000 h showing the formation of a ternary R phase. This image was not taken from the sample shown in Fig. 7.7(b), but a sister sample cut from the same diffusion multiple.

The EPMA data from another scan (scan #19 in Fig. 7.7(b), from left to right) are plotted in both composition–distance and composition–composition formats in Fig. 7.12. In this case, the extrapolation of the σ phase compositions using the composition–distance plot is difficult, but relatively straightforward for the composition–composition plot with the heavy dotted lines shown in Fig. 7.12(b).

A final example of tie-line data extraction is shown in Fig. 7.13 for a scan started in the R phase, crossed the σ phase, and ended in the fcc phase (scan #6 in Fig. 7.7(b), from top to bottom). It is difficult to decide whether the data in the first 15 μm of Fig. 7.13(a) are from a single-phase region with smoothly varying Cr and Mo concentrations or two separate phases (R and σ). The composition–composition plot in Fig. 7.13(b) clearly shows the tie-line information.

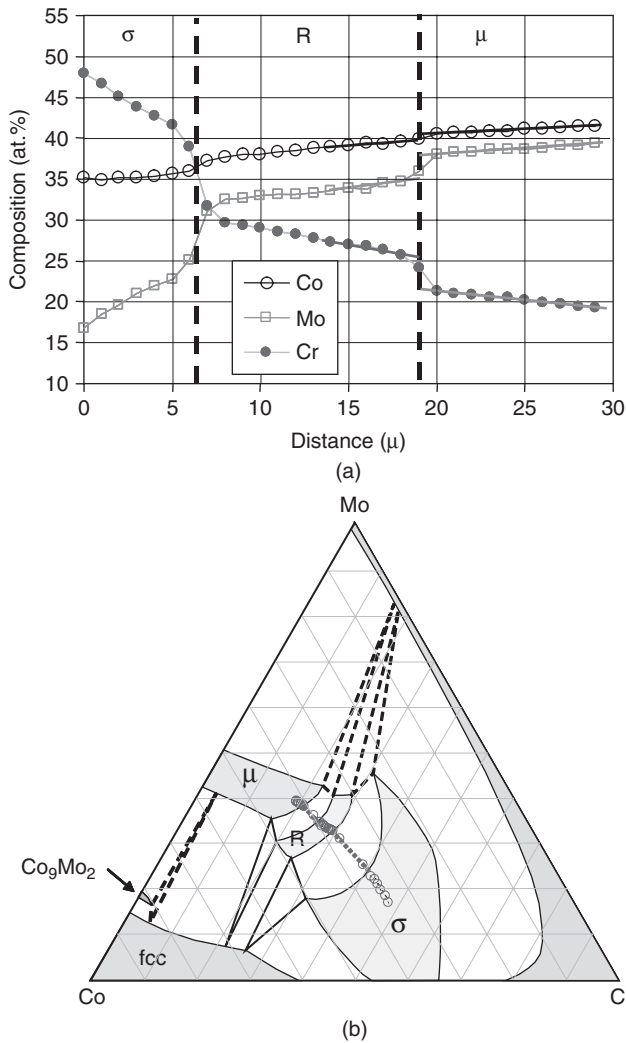


Figure 7.11 Plots used to extract equilibrium tie lines from an EPMA scan that started in the σ phase, crossed the R phase, and ended in the μ phase (scan #16 in Fig. 7.7(b), from right to left): (a) plot of compositions of the elements in at.% against distance and (b) plot of the at.% Mo against at.% Cr onto an isothermal section, showing the tie-line compositions at the end of the heavy dotted lines.

The examples in Figs. 7.11–7.13 clearly show the usefulness of composition–composition plots in tie-line data extraction. Sometimes, one needs the composition–distance plot together with a BSE image to define the tie lines and phase boundaries. This is especially true when the compositions of the two phases are very close.

By performing analyses similar to that shown in Figs. 7.11–7.13, lots of tie lines were obtained to construct the equilibrium isothermal section of the Co–Cr–Mo

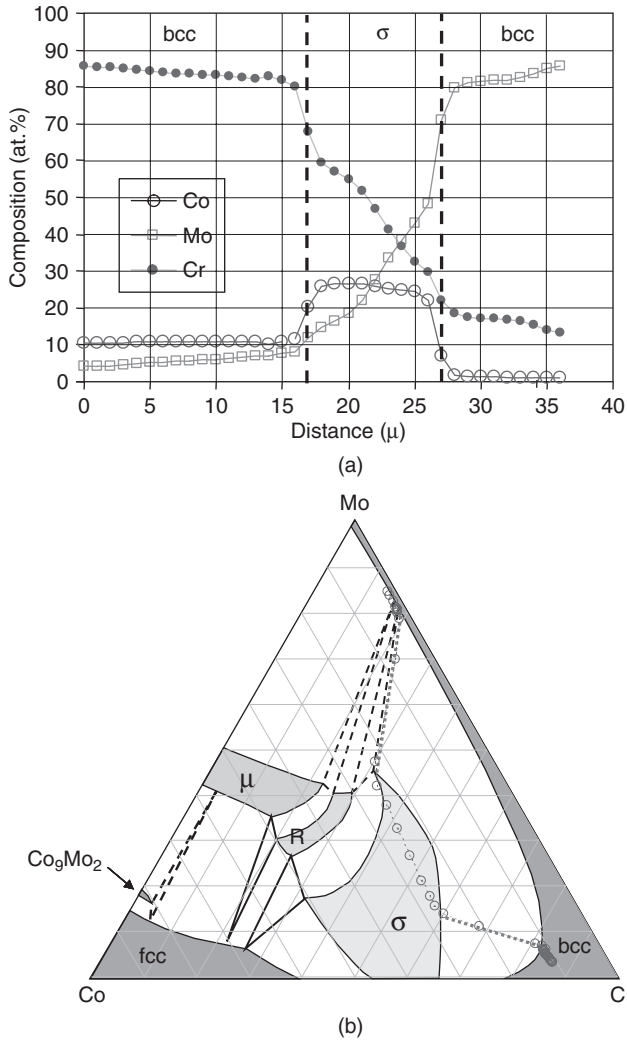


Figure 7.12 Plots used to extract equilibrium tie lines from an EPMA scan that started in the Cr-rich bcc phase, crossed the σ phase, and ended in the Mo-rich bcc phase (scan #19 in Fig. 7.7(b), from left to right): (a) plot of compositions of the elements in at.% against distance and (b) plot of the at.% Mo against at.% Cr onto an isothermal section, showing the tie-line compositions at the end of the heavy dotted lines.

ternary system (Fig. 7.14). The three-phase tie-triangles are obtained by extrapolating the related three two-phase region tie lines.

Since large amounts of EPMA data are generated during the analysis of the diffusion multiple, automated plotting procedures have been developed based on Microsoft Excel Spreadsheet and MatLab software. These programs helped to reduce the data extraction time from days to hours.

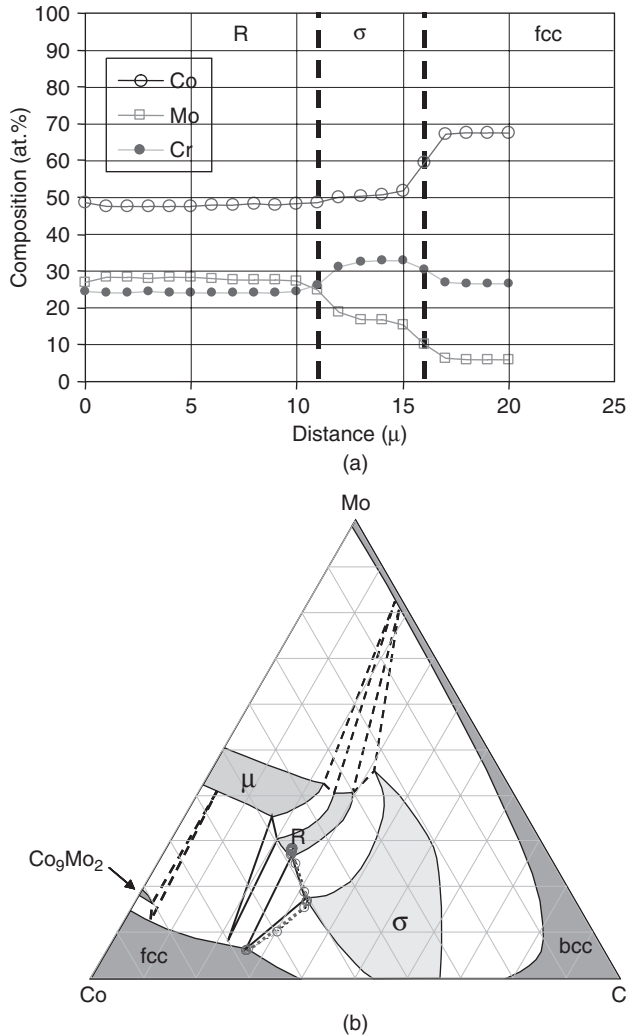


Figure 7.13 Plots used to extract equilibrium tie lines from an EPMA scan that started in the R phase, crossed the σ phase, and ended in the fcc phase (scan #6 in Fig. 7.7(b), from top to bottom): (a) plot of compositions of the elements in at.% against distance and (b) plot of the at.% Mo against at.% Cr onto an isothermal section, showing the tie-line compositions at the end of the heavy dotted lines.

4 SOURCES OF ERRORS

The local equilibrium at the phase interfaces is the basis for using diffusion multiples to map phase diagrams. The existence of such local equilibrium and its reliability in establishing equilibrium tie-line information has been demonstrated for many years in diffusion couples [6,7]. One can refer to the discussion of this topic in Chapter 6 of this book.

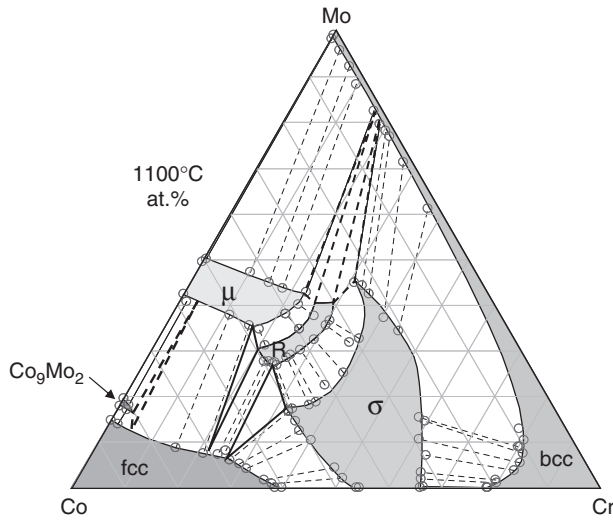


Figure 17.14 The 1100°C isothermal section of the Co–Cr–Mo ternary system determined from the diffusion multiple shown in Fig. 7.1 that was annealed at 1100°C for 1000 h. The phase diagram is plotted in at.% axes with the scales from 0% to 100% for each element removed for simplicity.

For each tie line, we can only obtain one set of data from one polished cross-section of a diffusion multiple. This is different from analysis of individual alloy samples from which several repeats can be made for a single tie line. Fortunately, the consistency of the tie line trends in the diffusion-multiple results (e.g., Fig. 7.14) gives as much confidence as that from repeated results from individual alloys.

The major source of error lies in the interpretation and extraction of equilibrium tie lines from EPMA results. There is lots of information condensed in a very small area of a sample, and one cannot practically perform EPMA analysis at every location in the interdiffusion zone. It is not even practical to use very small steps such as 1 μm for all the scans. One can fail to detect phases that are actually there, simply by performing the EPMA line scans at step sizes that are too large.

It is very convenient for EPMA experiments and also for automated data reduction to arrange the EPMA line scans along either the X or Y directions, as in the examples in Figs. 7.4(c) and 7.7(b). Sometimes, such a scan traverses an interphase interface at an angle not perpendicular to the interface, for example, line scan #19 in Fig. 7.7(b). If the compositional gradient is very steep at that location, the corresponding tie line extracted may not be the real tie line, but at an angle with it. This can be found out by examining the consistency of the tie-line orientation and by examining whether tie-line crossing is observed. For instance, a slight tie-line crossing is observed for the $\sigma + \text{bcc}$ two-phase region in Fig. 7.14. When this happens, the related “tie lines” should be regarded as less reliable data comparing to others. Fortunately, many state-of-the-art EPMA systems allow titled line scans to reduce such a problem.

On rare occasions, one of the phases may not form by interdiffusion reaction in diffusion couples, which makes one wonder whether a similar situation might happen in diffusion multiples. A famous example is the Ti–Al binary system [23]. When

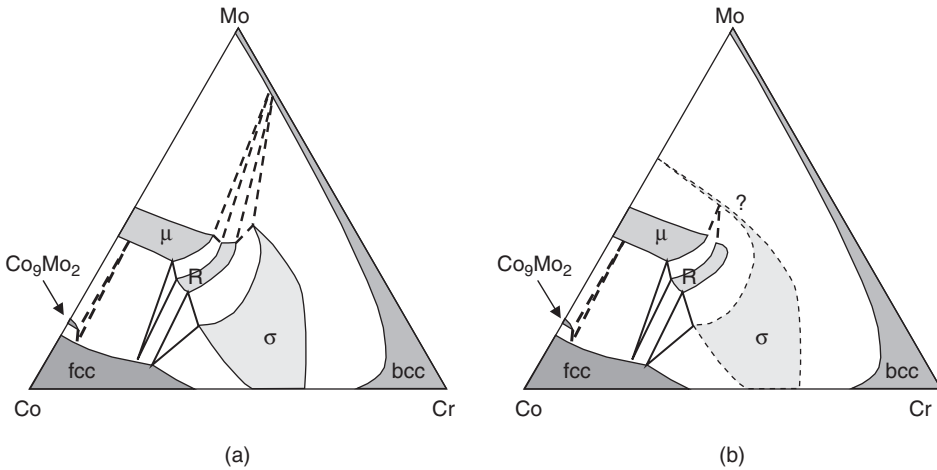


Figure 7.15 Schematic Co–Cr–Mo isothermal sections at 1100°C showing the two possibilities regarding the stability of the σ phase: (a) current version of the phase diagram in which the σ phase in the Co–Mo binary system is unstable at 1100°C and (b) a plausible isothermal section at 1100°C if the σ phase is stable at this temperature. The schematic phase diagrams are plotted in at.% axes with the scales from 0% to 100% for each element removed for simplicity.

Ti/Al diffusion couples were made, only the TiAl_3 phase was found, but when Ti/TiAl₃ diffusion couples were made, all the compounds appeared [23]. A close examination of the cases reported with missing phases in diffusion couples shows that in most such cases equilibration was attempted at temperatures below half of the homologous melting points, although the exact reason for the absence of phases under these conditions is still not well understood. All the recent phase diagram determination work using diffusion multiples has been concentrated on high temperatures. That may be the reason that we have not seen a missing phase situation. Even though the absence of phases was very rare, when using diffusion couples and diffusion multiples in determining phase diagrams one should always be watchful for the possibility of missing phases (especially at low temperatures). The absence of the σ phase in the Co–Mo binary diffusion couple discussed in Fig. 7.9 is consistent with the result of Quinn and Hume-Rothery [21] who observed the eutectoid decomposition of the σ phase at $\leq 1250^\circ\text{C}$, but contradict with the result of Heijwegen and Rieck [22] who reported the formation of the σ phase in a 1000°C annealed diffusion couple. If the result of Heijwegen and Rieck were repeated in the future, then a missing phase situation would have appeared. The 1100°C isothermal section of the Co–Cr–Mo would be look like Fig. 7.15(b). Since the σ phase has already formed in the Co–Cr binary system and the Co–Cr–Mo ternary system in the same diffusion multiple, it is hard to believe that it is a missing phase situation for the Co–Mo binary. Thus, the phase diagram reported in Figs. 7.14 and 7.15(a) are very likely the equilibrium isothermal section at 1100°C of the Co–Cr–Mo system.

One can reduce the chances of error by carefully following these tips:

- Perform the diffusion annealing at a high enough temperature to grow the phases to sufficiently large physical dimensions for reliable phase examination and

EPMA analysis. Thin phases or phases in small dimensions can be missed during analysis.

- Become familiar with the related binary systems and the ternary systems by carefully studying the literature information. It is very important to check all the reported phases and their stability ranges.
- Make sure all the phases are carefully checked with EBSD. It is important to make sure all the phases in the related binary systems are formed in the diffusion multiple, and any ternary phases reported in the literature for the particular ternary system are also present. High quality and high contrast BSE images are very useful in revealing the phases, especially when combined with EDS, optical microscopy and EBSD.
- Examine multiple pieces of the same diffusion multiple to make sure the phases are not inadvertently removed during sample preparation. Occasionally, a brittle phase may fall out of the sample during cutting, grinding, or polishing. One needs to investigate the cracks and porosities in the tri-junction areas to make sure they are not the results of phases that have been removed during specimen preparation. This can be done by examining the same location for different slices of the same diffusion multiple.
- Correlate the EPMA results and BSE images with EBSD results for consistency. If inconsistency is found, one needs to examine whether the interpretation of the EPMA results is correct. Automation in data extraction is a great means to save time, but one needs to be watchful to make sure it does not introduce error.
- Use equilibrated alloys to check regions of the phase diagrams in doubt. This is especially important for complex phase diagrams with multiple phases. In case the funding situation wouldn't allow the making of individual alloys, the regions in doubt should only be reported as tentative results. For instance, the two three-phase regions $bcc + \mu + R$ and $bcc + R + \sigma$ in Fig. 7.14 are reported as tentative results as indicated by the dashed lines.

5 CONCLUDING REMARKS

The best way to check the reliability of the diffusion-multiple approach is to compare the phase diagrams obtained from diffusion multiples to those obtained from equilibrated alloys and diffusion couples. A careful comparison for many systems has been performed [6]. The excellent agreements demonstrate that diffusion multiples can be used to determine phase diagrams at orders of magnitude increases in efficiency without sacrificing the quality of the data. A comparison of results for three ternary systems is shown in Figs. 7.16 and 7.17 [1,2,13,24,25]. The good agreement is very apparent.

The combination of the use of diffusion multiples with results on selected equilibrated alloys would be a good safety check against any potential occurrences of metastable or missing phases. Phase diagrams mapped at two or more temperatures are also very useful to check the consistency and reliability of the results.

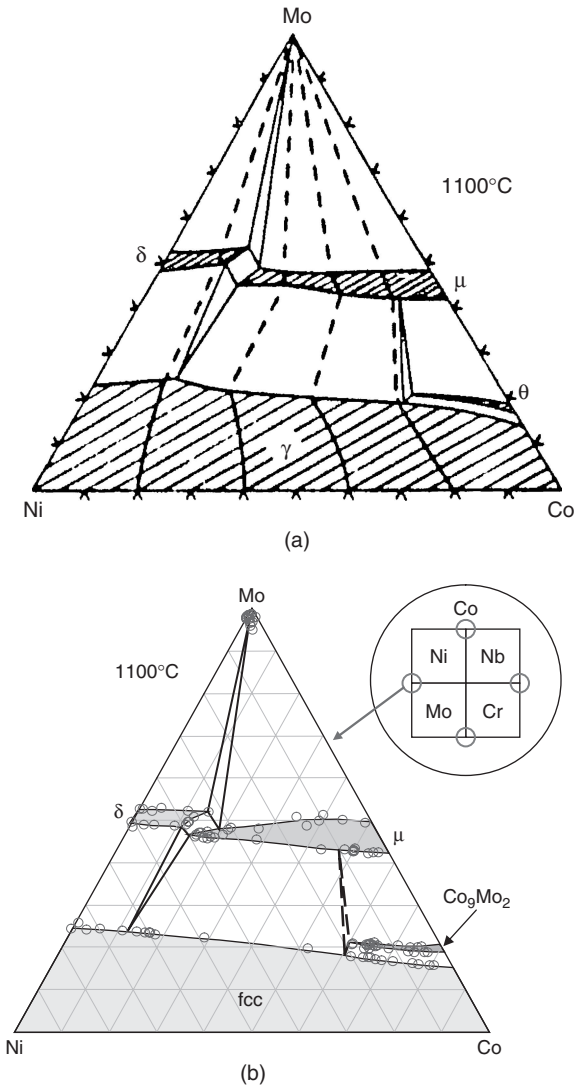


Figure 7.16 Comparison of the 1100°C isothermal section of the Co–Mo–Ni ternary system: (a) results obtained from nine equilibrated alloys and eight diffusion couples [24] and (b) results obtained from the diffusion multiple shown in Fig. 7.1.

No method is foolproof for phase diagram determination. One needs to be watchful for potential pitfalls for each method, including the diffusion-multiple method. The biggest source of error lies in the interpretation of extracted tie-line information. By following the suggestions discussed in this chapter, one can reliably determine phase diagrams using the diffusion-multiple approach, taking full advantage of its efficiency while maintaining the high quality of results.

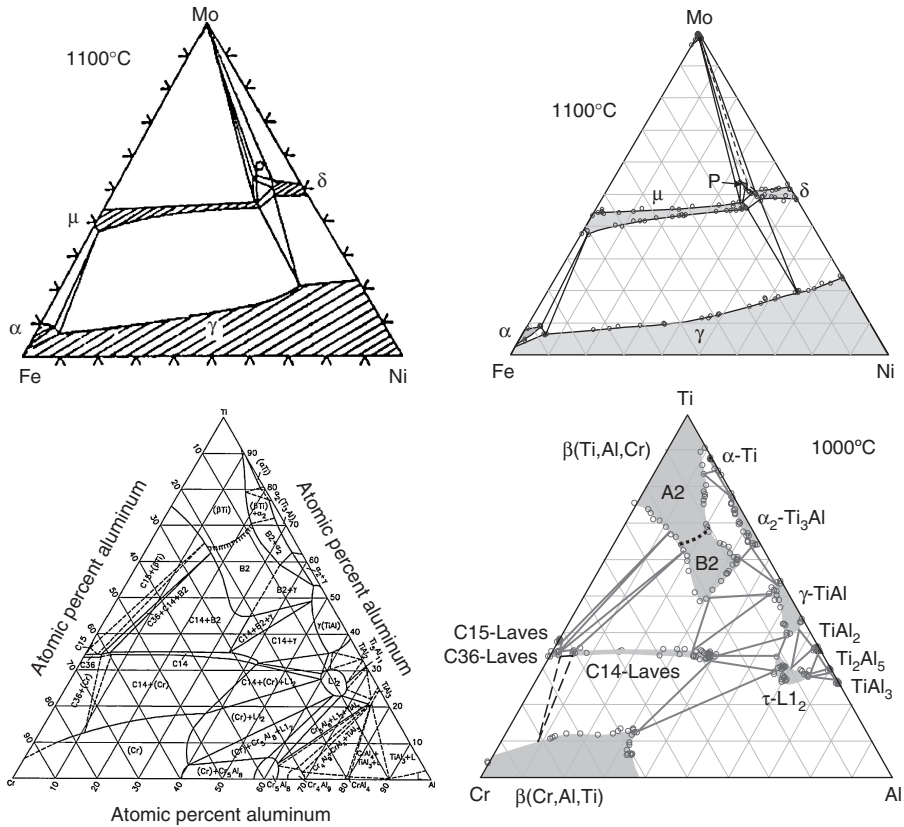


Figure 7.17 Comparison of phase diagrams determined from diffusion multiples with those obtained from equilibrated alloys and diffusion couples: (a) the 1100°C isothermal section of the Fe–Mo–Ni ternary system obtained from equilibrated alloys and diffusion couples [24]; (b) the 1100°C isothermal section of the Fe–Mo–Ni ternary system obtained from a diffusion multiple [1,2]; (c) the 1000°C isothermal section of the Al–Cr–Ti ternary system obtained from more than 100 equilibrated alloys [25]; and (d) the 1000°C isothermal section of the Al–Cr–Ti ternary system obtained from a single diffusion multiple [13].

ACKNOWLEDGMENTS

The author is grateful to L.N. Brewer, E.L. Hall, M.F. Henry, M.R. Jackson, L.A. Peluso, A.M. Ritter, and J.H. Westbrook for their help and/or valuable discussions. Special appreciation is extended to L.A. Peluso for an elegant description of EPMA in Section 3.2. Various parts of the work were supported by General Electric (GE) Company internal funding, the US Air Force Office of Scientific Research (AFOSR) under grant number F49620-99-C-0026 with C. Hartley as a program manager; and Defense Advanced Research Projects Agency (DARPA) under the Accelerated Insertion of Materials (AIM) program (Grant number: F33615-00-C-5215) with Dr. L. Christodoulou as the project manager and Dr. R. Dutton as the

project monitor. I am especially thankful to my wife, Felicia for her understanding and tolerance during the manuscript preparation.

REFERENCES

1. J.-C. Zhao, *Adv. Eng. Mater.*, 3 (2001) 143.
2. J.-C. Zhao, *J. Mater. Res.*, 16 (2001) 1565.
3. J.-C. Zhao, M.R. Jackson, L.A. Peluso and L. Brewer, *MRS Bull.*, 27 (2002) 324.
4. J.-C. Zhao, *Annu. Rev. Mater. Res.*, 35 (2005) 51.
5. J.-C. Zhao, *Prog. Mater. Sci.*, 51 (2006) 557.
6. A.D. Romig, *Bull. Alloy Phase Diagr.*, 8 (1987) 308.
7. F.J.J. van Loo, *Prog. Solid State Chem.*, 20 (1990) 47.
8. M. Hasebe and T. Nishizawa, in G.C. Carter (ed.), *Application of Phase Diagrams in Metallurgy and Ceramics*, Vol. 2, NBS Special Publications, No. 496, Gaithersburg, MD, 1978, p. 911.
9. Z. Jin, *Scand. J. Metall.*, 10 (1981) 279.
10. J.-C. Zhao and Z. Jin, *Z. Metallkde.*, 81 (1990) 247.
11. Z. Jin and C. Qiu, *Metall. Mater. Trans.*, 24A (1993) 2137.
12. J.-C. Zhao, M.R. Jackson, L.A. Peluso and L.N. Brewer, *JOM*, 54(7) (2002) 42.
13. J.-C. Zhao, *J. Mater. Sci.*, 39 (2004) 3913.
14. F.J. Humphreys, *Scripta Mater.*, 51 (2004) 771.
15. D.J. Dingley and V. Randle, *J. Mater. Sci.*, 27 (1992) 4545.
16. A.J. Schwartz, M. Kumar and B.L. Adams (eds.), *Electron Backscatter Diffraction in Materials Science*, Kluwer Academic/Plenum, New York, 2000.
17. T.B. Massalski (ed.), *Binary Alloy Phase Diagrams*, 2nd edn, ASM International, Materials Park, OH, 1990.
18. V.D. Scot and G. Love, in V.D. Scot and G. Love (eds.), *Quantitative Electron-Probe Microanalysis*, Ellis Horwood Ltd., Great Britain, 1983, p. 32.
19. J.I. Goldstein, D.E. Newbury, P. Echlin, D.C. Joy, A.D. Romig, C.E. Lyman, C. Fiori and E. Lifshin (eds.), *In Scanning Electron Microscopy and X-ray Microanalysis*, Plenum Press, New York, 1981, p. 111.
20. J.T. Armstrong, *Proceedings of the Annual MSA/MAS Meeting*, 1999 p. 561.
21. T.J. Quinn and W. Hume-Rothery, *J. Less-Common Met.*, 5 (1963) 314.
22. C.P. Heijwegen and G.D. Rieck, *J. Less-Common Met.*, 34 (1974) 309.
23. F.J.J. van Loo and G.D. Rieck, *Acta Metall.*, 21 (1973) 61.
24. F.J.J. van Loo, G.F. Bastin, J.W.Q.A. Vrolijk and J.J.M. Hendriks, *J. Less-Common Met.*, 72 (1980) 225.
25. V. Raghavan, *J. Phase Equilib. Diff.*, 26 (2005) 349.